AGU PUBLICATIONS

Geophysical Research Letters

RESEARCH LETTER
10.1002/2016GL070033

Special Section:
First results from NASA's Magnetospheric Multiscale (MMS) Mission

MMS observations of ion-scale magnetic island in the magnetosheath turbulent plasma

S. Y. Huang[1,2], F. Sahraoui[2], A. Retino[2], O. Le Contel[2], Z. G. Yuan[1], A. Chasapis[3], N. Aunai[2], H. Breuillard[2], X. H. Deng[4], M. Zhou[5], H. S. Fu[6], Y. Pang[4], D. D. Wang[1], R. B. Torbert[7], K. A. Goodrich[8], R. E. Ergun[8], Y. V. Khotyaintsev[9], P.-A. Lindqvist[10], C. T. Russell[11], R. J. Strangeway[11], W. Magnes[12], K. Bromund[13], H. Leinweber[11], F. Plaschke[12], B. J. Anderson[13], C. J. Pollock[14], B. L. Giles[14], T. E. Moore[14], and J. L. Burch[15]

[1]School of Electronic Information, Wuhan University, Wuhan, China, [2]Laboratoire de Physique des Plasmas, CNRS-Ecole Polytechnique-UPMC, Palaiseau, France, [3]Bartol Research Institute and Department of Physics and Astronomy, University of Delaware, Newark, Delaware, USA, [4]Institute of Space Science and Technology, Nanchang University, Nanchang, China, [5]Department of Physics and Astronomy, University of California, Los Angeles, California, USA, [6]School of Space and Environment, Beihang University, Beijing, China, [7]Department of Physics, University of New Hampshire, Durham, New Hampshire, USA, [8]LASP, University of Colorado Boulder, Boulder, Colorado, USA, [9]Swedish Institute of Space Physics, Uppsala, Sweden, [10]Royal Institute of Technology, Stockholm, Sweden, [11]Department of Earth, Planetary, and Space Sciences, University of California, Los Angeles, California, USA, [12]Space Research Institute, Austrian Academy of Sciences, Graz, Austria, [13]Johns Hopkins University Applied Physics Laboratory, Laurel, Maryland, USA, [14]NASA, Goddard Space Flight Center, Greenbelt, Maryland, USA, [15]Southwest Research Institute, San Antonio, Texas, USA

Key Points:
- Ion-scale magnetic island is identified in the magnetosheath
- Electron beams and intense wave emissions in the magnetic island
- Multiscale coupling occurs in magnetic island

Correspondence to:
S. Y. Huang,
shiyonghuang@whu.edu.cn

Citation:
Huang, S. Y., et al. (2016), MMS observations of ion-scale magnetic island in the magnetosheath turbulent plasma, *Geophys. Res. Lett.*, *43*, 7850–7858, doi:10.1002/2016GL070033.

Received 14 JUN 2016
Accepted 26 JUL 2016
Accepted article online 29 JUL 2016
Published online 14 AUG 2016

Abstract In this letter, first observations of ion-scale magnetic island from the Magnetospheric Multiscale mission in the magnetosheath turbulent plasma are presented. The magnetic island is characterized by bipolar variation of magnetic fields with magnetic field compression, strong core field, density depletion, and strong currents dominated by the parallel component to the local magnetic field. The estimated size of magnetic island is about 8 d_i, where d_i is the ion inertial length. Distinct particle behaviors and wave activities inside and at the edges of the magnetic island are observed: parallel electron beam accompanied with electrostatic solitary waves and strong electromagnetic lower hybrid drift waves inside the magnetic island and bidirectional electron beams, whistler waves, weak electromagnetic lower hybrid drift waves, and strong broadband electrostatic noise at the edges of the magnetic island. Our observations demonstrate that highly dynamical, strong wave activities and electron-scale physics occur within ion-scale magnetic islands in the magnetosheath turbulent plasma.

1. Introduction

The magnetosheath is the region downstream of bow shock that lies between the bow shock and the magnetopause. The magnetosheath is a highly turbulent region where plasma instabilities [*Schwartz et al.*, 1996; *Lucek et al.*, 2005; *Sahraoui et al.*, 2004], current sheets associated with magnetic reconnection [*Retinó et al.*, 2007; *Phan et al.*, 2007; *Chasapis et al.*, 2015], turbulent electromagnetic field fluctuations [*Sahraoui et al.*, 2003, 2006; *Huang et al.*, 2014a; *Hadid et al.*, 2015], and Alfvén vortex filaments [*Alexandrova et al.*, 2008] have been reported. Numerical simulations have shown that magnetic reconnection can take place in thin current sheets that form in turbulent plasmas due to different coherent structures, such as magnetic islands and magnetic holes [e.g., *Karimabadi et al.*, 2013; *Roytershteyn et al.*, 2015]. Recent global hybrid and fully kinetic simulations have shown that magnetic islands can form in the quasi-parallel magnetosheath because of the enhanced level of the turbulent fluctuations in it, in comparison with the quasi-perpendicular magnetosheath [*Karimabadi et al.*, 2014]. The reported magnetic islands were observed from shock surface to the vicinity of the magnetopause, had a spatial size of a few tens of ion inertial length in the magnetosheath, and were characterized by a density depletion and magnetic field compression [*Karimabadi et al.*, 2014, Figures 6, 9, and 13]. In the magnetosheath, magnetic islands are distinct from flux transfer events (FTEs) because FTEs are generated during magnetic reconnection at the magnetopause and some magnetic field lines are still connected to the Earth [e.g., *Elphic*, 1995; *Roux et al.*, 2015]. In spacecraft data, distinguishing between magnetic islands and flux ropes is not obvious (magnetic islands can indeed be seen as the 2-D version of 3-D flux ropes [e.g., *Fu et al.*, 2015, 2016]). For convenience, we will use the terminology of "magnetic islands" in the remainder of this paper.

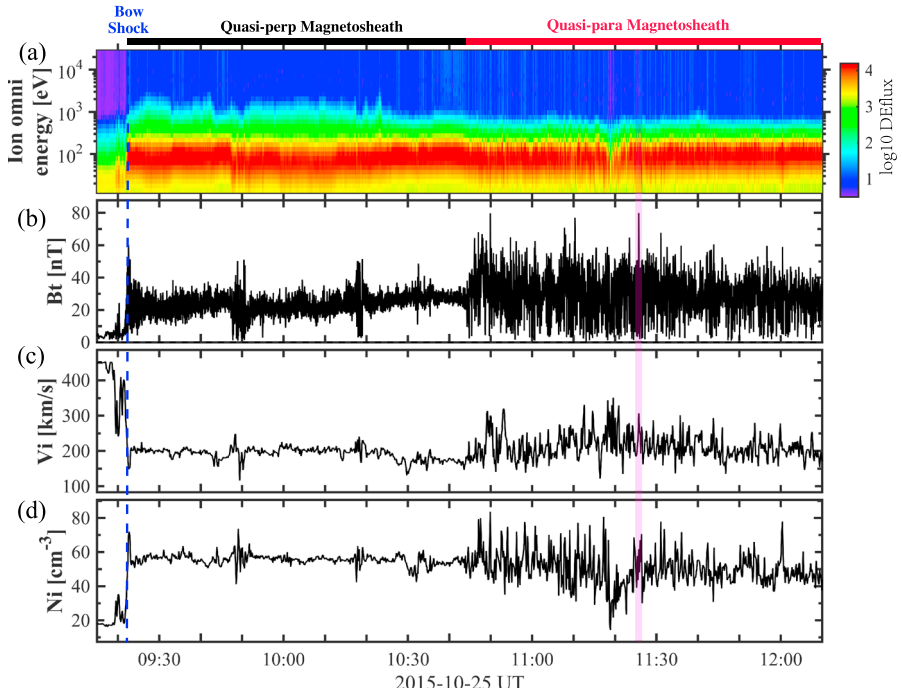

Figure 1. Overview of MMS observations. (a) Ion differential energy flux, (b) magnitude of the magnetic field, (c) amplitude of ion velocity, and (d) ion density. The crossing of bow shock is marked by a blue dashed line. The analyzed magnetic island is indicated by the pink shaded region.

Magnetic islands associated with magnetic reconnection are frequently observed in the magnetotail [e.g., *Slavin et al.*, 2003a; *Huang et al.*, 2012a, 2014b, 2016]. However, in a turbulent medium such as the magnetosheath, the search for magnetic islands in spacecraft data becomes more difficult because their motions can be in any direction of space due to the turbulent state of the medium (unlike in the magnetotail where they move essentially in the X_{GSM} direction). So far, because of the limited time resolution of the plasma data on board previous space missions, studies of small (ion-scale) magnetic islands have not been possible. In this letter, thanks to the unprecedented high time resolution data of the Magnetospheric Multiscale (MMS) mission [*Burch et al.*, 2015], we report the first observations of ion-scale magnetic islands in the magnetosheath and study their dynamics.

2. Observations

In this work, we use the fields data from the Fluxgate Magnetometer [*Russell et al.*, 2014], the Search-Coil Magnetometer (SCM) [*Le Contel et al.*, 2014], the Electric Double Probe [*Torbert et al.*, 2014; *Lindqvist et al.*, 2014; *Ergun et al.*, 2014], and the 3-D particle data (distribution function and plasma moments) from the Fast Plasma Instrument [*Pollock et al.*, 2016].

Figure 1 displays an overview of plasma and magnetic field observations on 25 October 2015. MMS crossed the bow shock around 09:21 UT and then entered into the magnetosheath. Between 09:21 and 10:43 UT, MMS crossed the magnetosheath downstream of quasi-perpendicular shock, before entering into the quasi-parallel magnetosheath region about 10:30. This region is characterized by stronger fluctuations in the magnetic field, the ion velocity, and the plasma density in comparison with the quasi-perpendicular magnetosheath (see Figures 1b–11d). We identified a lot of magnetic islands in the highly turbulent quasi-parallel magnetosheath. Here we analyzed one of them in detail, which is denoted by the pink shaded region in Figure 1.

Figure 2 shows the detailed observations of the magnetic island from 11:25:42 UT to 11:25:45 UT. During this time interval, all instruments were in burst mode, and the MMS spacecraft had a tetrahedral configuration with a separation of ~12 km. In this study, and unless otherwise stated, all the data are presented in local boundary normal coordinates (often abbreviated as LMN), which were determined by the minimum variance

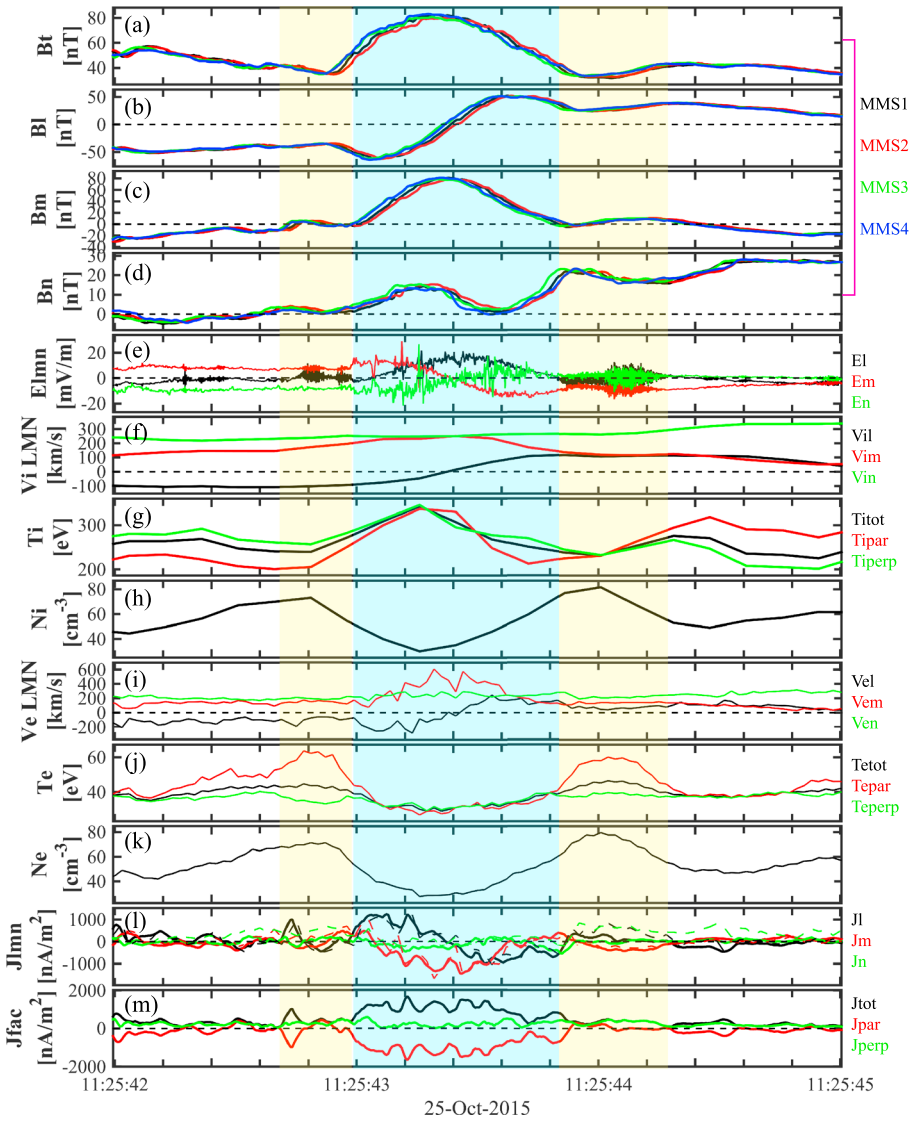

Figure 2. Detailed observations of the magnetic island in the magnetosheath (vector data are given in LMN coordinates). (a–d) Magnitude and components of the magnetic field from the four MMS spacecraft. (e) Electric field, (f) three components of ion velocity, (g) ion temperature, (h) ion density, (i) electron velocity, (j) electron temperature, (k) electron density, (l) current density calculated using the curlometer method (solid lines) and the plasma measurements (dashed lines), and (m) current in field-aligned coordinates. The data shown in Figures 2e–2m are measured by MMS2. The center (respectively, edges) of the magnetic island is marked by the shaded yellow (respectively, blue) regions.

analysis of the magnetic fields [*Sonnerup and Scheible*, 1998]. In this coordinate system, *L* is the maximum variation direction, *N* is the minimum variation direction, and *M* completes a right-handed orthogonal coordinate system. Note that the *N* direction was found to be consistent with the normal direction inferred from the timing analysis of using the magnetic field data from the four MMS spacecraft. Figure 2b shows a clear bipolar variation in the B_L component (from negative to positive) around 11:25:43.40 UT on the four MMS spacecraft. It is accompanied by a peak in the B_M component (Figure 2c) and an enhancement in the total field B_{tot} (Figure 2a). These signatures are the three criteria used in this study to identify the magnetic islands, which are consistent with those used in previous works to identify similar structures at the magnetopause and in the magnetotail [e.g., *Elphic*, 1995; *Slavin et al.*, 2003a]. These criteria can rule out the possibility of O lines [e.g., *Eastwood et al.*, 2005]. Figures 2f and 2i show that the crossing of the magnetic island is accompanied with a reversal in the plasma flow components V_{iL} and V_{eL}. This indicates that the magnetic island was embedded in a vortex-like plasma flow, which may be seen as streamlines along the ambient magnetic field

in the LN plane. Furthermore, a plasma density depletion is detected inside the magnetic island (Figures 2h and 2k), along with an increase (respectively, a decrease) in the ion (respectively, electron) temperature (Figures 2g and 2k). Strong electric field (Figure 2e) shows a peak in the E_L component and a bipolar signature in the E_M and E_N components during the crossing of the magnetic island, which is mainly due to the convective electric field (not shown). Figures 2l and 2m show the current density calculated using the curlometer method [*Dunlop et al.*, 2002]. Current estimated by the plasma measurements (i.e., $J_{\mathrm{pla}} = ne(V_i - V_e)$, where n is the plasma density, e is the change, V_i is the ion flow, and V_e is the electron flow), is also displayed by dashed lines in Figure 2l. Both currents are very consistent with each other, indicating that the currents were well resolved during this time interval. Intense currents are observed in the magnetic island, with a strong axial current component (J_M). The parallel current inside the magnetic island is found to be much larger than the perpendicular one. This feature contrasts with most magnetic islands observed in the magnetotail shown to have a significant (sometimes dominant) perpendicular current [e.g., *Slavin et al.*, 2003b; *Walsh et al.*, 2007]. It is worth noting that there are large fluctuations in the electric field, along with an increase in the density and the electron temperature (with $T_{e\|} \gg T_{e\perp}$) at both edges of magnetic island. The observed electron anisotropy would provide free energy for plasma instabilities and wave generations observed here (see below for details). Timing analysis is used to estimate the speed of the magnetic island. It is found to move with a normal speed V_N~230 km/s, yielding an estimated width in the N direction $L_N \sim V_{\mathrm{N}} \times dt \sim 240$ km, where $dt = 1.06$ s is the duration of the crossing of magnetic island. The estimated size L_N is about 8 d_i, where d_i is the ion inertial length (d_i~30 km based on n~58 cm^{-3}).

Figure 3 shows the plasma observations associated with the identified magnetic island from MMS2. Inside the magnetic island, ion differential energy fluxes increase at the high-energy level (Figure 3b) but decrease at the low-energy level, yielding the ion density decreases and the ion temperature increases. In contrast, electron differential energy fluxes decrease at high- and low-energy levels (Figure 3c), yielding both the electron density and temperature decrease. The plasma behavior at both edges of the magnetic island contrasts with the one inside the magnetic island. Electron pitch angle distributions at three energy bands are presented in Figures 3d–3f. They show different pitch angle distributions inside and at the edges of the magnetic island. Bidirectional electron flows are clearly detected at the edges of the magnetic island, while a parallel electron flow at the energy level of 0–200 eV is observed in the center of magnetic island. As for Figure 3d, the fluxes from 2 to 30 keV are too low to be measured. The cuts at three times (marked by three red arrows at the bottom of Figure 3f) at pitch angles 0°, 90°, and 180° are shown in Figures 3g–33i. The cuts clearly show bidirectional electron beams in the energy range of 60–300 eV at the edges of the magnetic island (Figures 3g and 3i) and a parallel electron beam in the energy range of 30–120 eV inside the magnetic island (Figure 3h). These pitch angle distributions can provide free energy for the generation of the waves that we will discuss later.

Figures 4b and 4c display the power spectral densities of the electric and the magnetic fields associated with the magnetic island. Strong electric and magnetic wave activities around the lower hybrid frequency (f_{lh}) can be seen inside the magnetic island, which would be electromagnetic lower hybrid drift waves due to the large gradient in the plasma density (Figures 2h and 2k) in high plasma β ($\beta \geq 1$, not shown here) [e.g., *Zhou et al.*, 2014]. *Roytershteyn et al.* [2012] have found that lower hybrid drift instabilities are enhanced when the ratio between ion and electron temperature (T_i/T_e) is much smaller than 1. However, in our observation we found $T_i/T_e \gg 1$ during the crossing of the magnetic island (T_i~230–340 eV in Figure 2g and T_e~30–45 eV in Figure 2j), which suggests that the excited lower hybrid drift waves may be rather influenced by the density gradient as seen in Figures 2h and 2k. Whistler waves (marked by two dashed ellipses in Figure 4b) and strong electrostatic waves activities around the electron cyclotron frequency (f_{ce}) or the proton plasma frequency (f_{pi}) are detected at the edges of the magnetic island. We analyzed the filtered (500 Hz–3 kHz) electric field data using the minimum variance analysis, where the k vector direction is given by the maximum variance direction (because the electric field perturbations are parallel to k). The estimated angles between the wave vector k and the ambient magnetic field B_0 is about 20° (respectively, 8°) at the leading (respectively, trailing) edge of the magnetic island, implying that the electrostatic waves seen around f_{ce} (or f_{pi}) are field-aligned polarized and may belong to broadband electrostatic noise (BEN) or electrostatic quasi-monochromatic (EQM) waves [*Pickett et al.*, 2005; *Shin et al.*, 2006]. In addition, weak electromagnetic wave activities around f_{lh} are also detected at both edges, which may be caused by the density gradient [e.g., *Zhou et al.*, 2014].

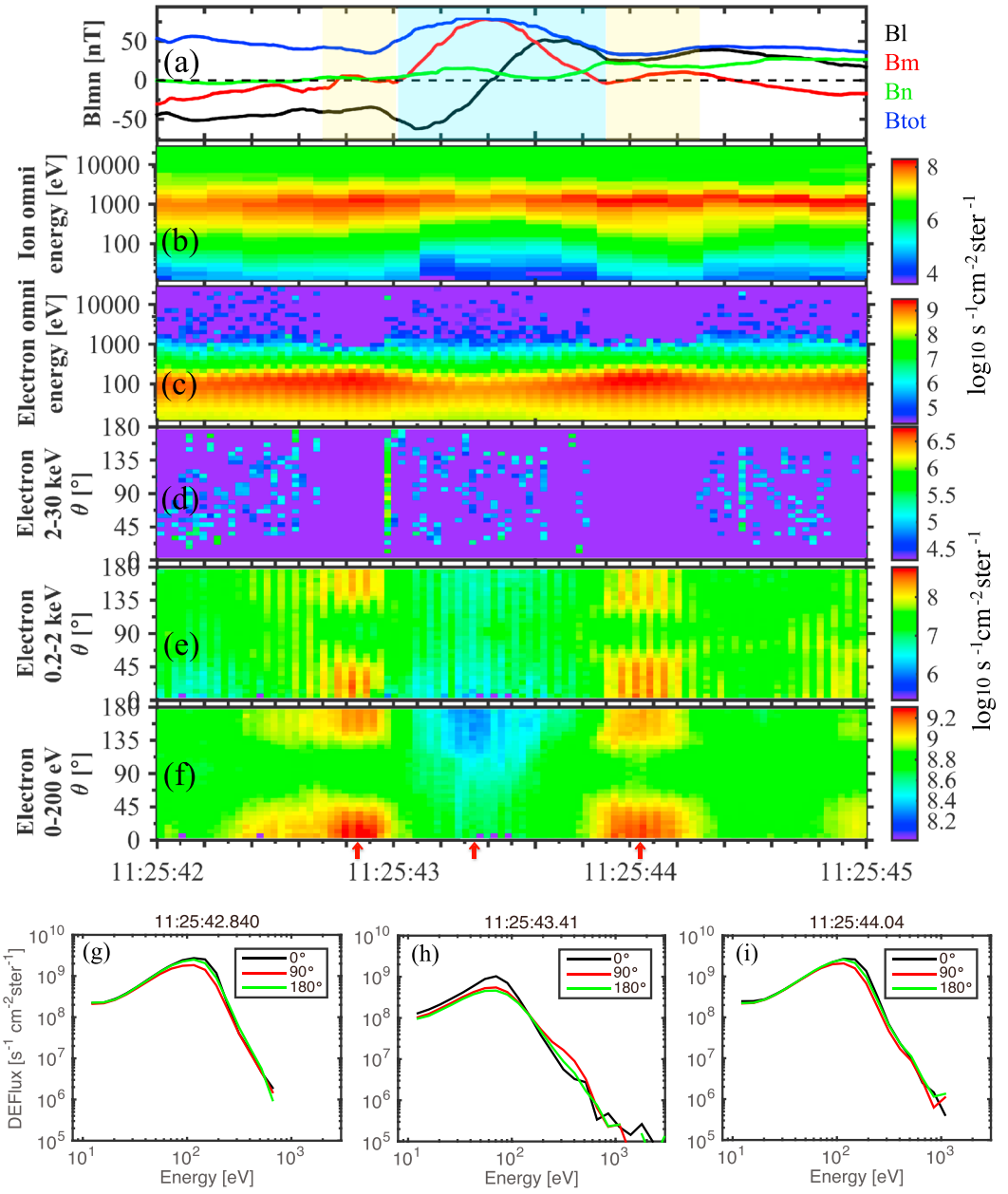

Figure 3. Particle observations of magnetic island in the magnetosheath. (a) Magnitude and three components of magnetic field in LMN coordinates; (b and c) ion and electron differential energy fluxes, respectively; (d–f) electron pitch angle distributions at high-, middle-, and low-energy levels; and (g–i) electron distributions at pitch angle 0°, 90°, and 180° during the three intervals marked by red arrows at the bottom of Figure 3f. The center (respectively, edges) of the magnetic island is marked by the shaded yellow (respectively, blue) regions.

Figure 4d presents the parallel electric field waveform. Large-amplitude waves (up to 40 mV/m) are located at both edges, which correspond to the electrostatic waves around f_{ce} (or f_{pi}) observed in Figure 4c. There is a series of electrostatic solitary waves (ESWs) inside the magnetic island that last less than 1 ms. They are characterized by a bipolar variation (from negative to positive or vice versa) in the parallel electric field component [e.g., *Pickett et al.*, 2003]. Figures 4e and 4f show the observations of ESWs inside the magnetic island from MMS1 and MMS2, respectively. The time intervals correspond to the black bars (for MMS1) and red bars (for MMS2) at the bottom of Figure 4d. Clear bipolar structures of ESWs lasting less than 1 ms and having amplitudes ranging from 0.4 mV/m to 6 mV/m are well measured inside the magnetic island.

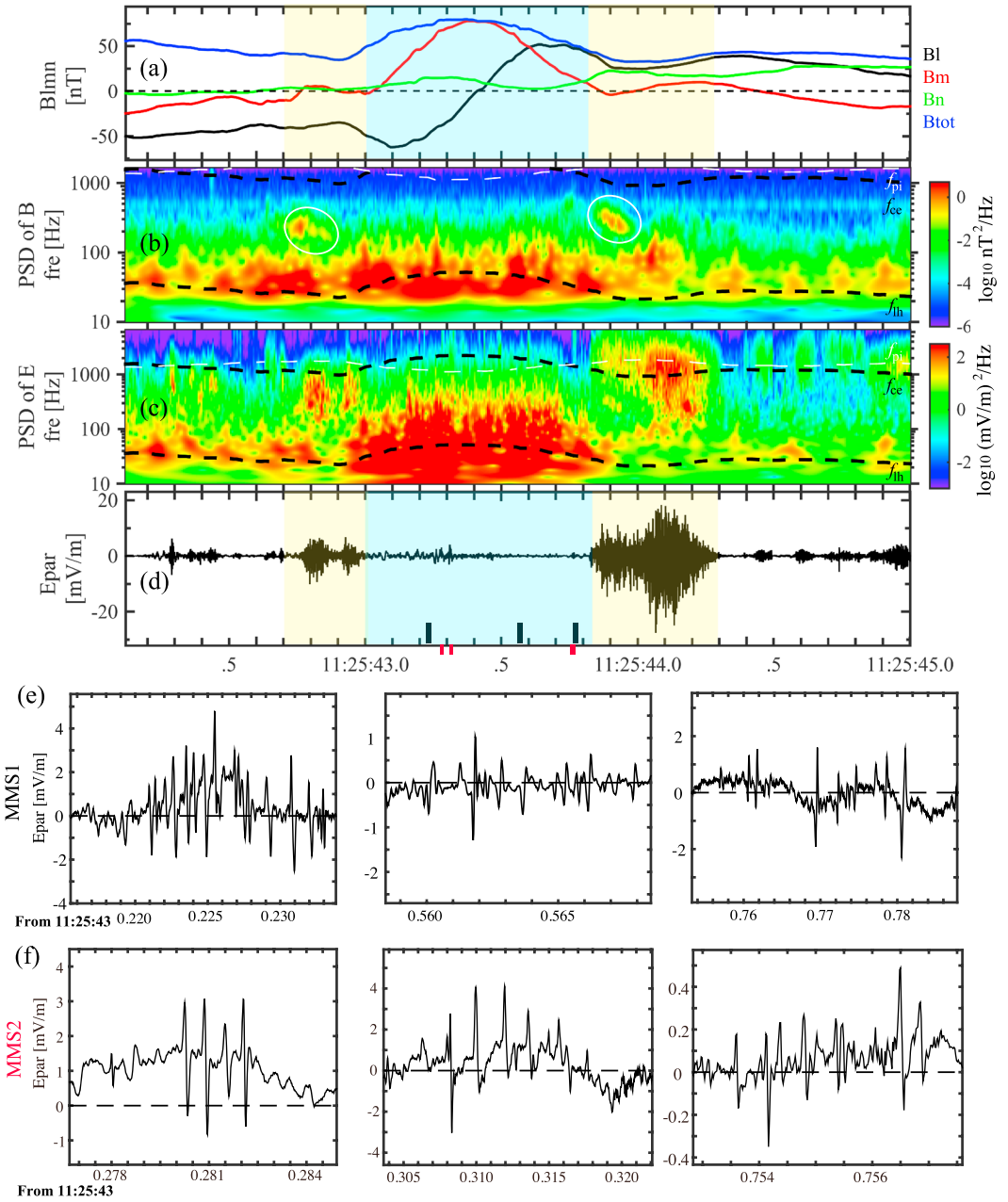

Figure 4. Waves observed in the magnetic island. (a) Magnitude and three components of magnetic field in LMN coordinates; (b and c) power spectral densities (PSDs) of the magnetic and electric field, respectively; (d) parallel electric field waveform from MMS2; and (e and f) zoomed-in parallel electric field, from MMS1 and MMS2, respectively, during the three time intervals marked by black and red bars at the bottom of Figure 4d from left to right. The center (respectively, edges) of the magnetic island is marked by the shaded yellow (respectively, blue) regions.

3. Discussion and Conclusions

MMS data have been used to identify magnetic islands in the turbulent magnetosheath. Our observations confirm the existence of several predicated features from numerical simulations [e.g., *Karimabadi et al.*, 2013, 2014], such as the complex interplay between coherent structures, strong wave activity, and particle heating.

Parallel current inside magnetic island was found to be dominant over the perpendicular one, implying that the magnetic island is close to a force-free configuration. Indeed, an estimation of the pressure gradient (not shown here) indicated that the magnetic island is close to a MHD equilibrium. This observation contrasts with

those reported in the magnetotail, where the magnetic islands were found to be either accelerating or braking due to external (nonequilibrium) forces [e.g., *Slavin et al.*, 2003b; *Walsh et al.*, 2007]. The nature of force-free configuration and its condition in the magnetic island will be studied in depth in the future.

ESWs were frequently observed in the magnetosheath [e.g., *Pickett et al.*, 2003, 2005] and near-magnetic reconnection sites in the magnetotail [e.g., *Khotyaintsev et al.*, 2010]. There are several mechanisms proposed in the literatures to explain the generation of ESWs, e.g., normal Buneman instability [*Buneman*, 1958], electron beam instability [e.g., *Omura et al.*, 1996], and nonlinear lower hybrid Buneman instability in the presence of an electron beam [*Jovanovic and Shukla*, 2004]. In our study, the appearance of the parallel electron beam inside the magnetic island (energy ~80 eV; Figure 3h), intense lower hybrid drift waves, and ESWs suggest that the observed ESWs may be generated by the beam-plasma instability or the lower hybrid Buneman instability. This is in agreement with *Graham et al.* [2016], who confirmed that the electrostatic instabilities driven by an electron beam (below 100 eV), namely, the beam-plasma instability, can generate ESWs (see Figure 13f therein and Figure 3h above).

Shin et al. [2006] have reported that EQM waves can be generated by the destabilization of the electron acoustic mode in the presence of electron beams. In our study, we have observed bidirectional electron beams at both edges of the magnetic island, which is similar to the electron observations in *Shin et al.* [2006]. Such electron beams may explain the generation of the EQM (or BEN) waves observed around f_{ce} (or f_{pi}) in our data that can also belong to electron acoustic mode [e.g., *Gary and Tokar*, 1985; *Shin et al.*, 2006]. We note that the ion acoustic mode can be ruled out from our observations considering the low-temperature ratio T_e/T_i~0.16, which is not consistent with the theoretical generation condition for ion acoustic mode, i.e., $T_e/T_i \gg 1$ as discussed in *Shin et al.* [2006].

On the other hand, whistler waves are known to be generated by electron temperature anisotropy $T_{e\perp} > T_{e\parallel}$ [e.g., *Gary and Karimabadi*, 2006; *Huang et al.*, 2012b] or electron beams via electron cyclotron resonance [*Zhang et al.*, 1999]. Recent kinetic simulations have shown that whistler waves can be generated in a reconnection separatrix region due to the beam whistler instability [*Fujimoto*, 2014]. In our data, we observed electron temperature anisotropy $T_{e\parallel} \gg T_{e\perp}$ and bidirectional electron beams. Moreover, the velocity of the resonant electrons is roughly estimated to $\sim 9.0 \times 10^3$ km/s (i.e., 230 eV), which is close to the energy peak of the electrons at the edges of magnetic island (Figures 3g and 3i). This suggests that the observed whistler waves could have been generated by the electron beam instability.

In summary, we presented the observations of ion-scale magnetic islands in the magnetosheath turbulent plasma. Their observational features, such as magnetic field compression, density depletion, and their size, were consistent with the simulation results of *Karimabadi et al.* [2014]. Furthermore, our observations show highly structured, dynamical, and intense wave emissions within the magnetic island. Distinct particle behaviors and wave activities are observed inside and at the edges of the magnetic island. ESWs and strong electromagnetic lower hybrid drift waves were detected inside the magnetic island corresponding to a parallel electron beam, while whistler waves, weak electromagnetic lower hybrid drift waves, and strong electrostatic waves around f_{ce} (or f_{pi}) were observed at the leading and trailing edges of the magnetic island along with bidirectional electron beams. These observations demonstrate the existence of strong (electron scale) wave activity and its multiscale coupling to the highly dynamical ion-scale magnetic island in the turbulent magnetosheath. The wave identifications, wave generation conditions, and wave-particle interactions within the magnetic island will be addressed in detail in the future studies.

Acknowledgments
We thank the entire MMS team and instrument leads for the data access and support. This work was supported by the National Natural Science Foundation of China (41374168 and 41404132), Program for New Century Excellent Talents in University (NCET-13-0446), and China Postdoctoral Science Foundation Funded Project (2015 T80830). S.Y.H. and F.S. acknowledge the financial support from the project THESOW, grant ANR-11-JS56-0008, and from LABEX Plas@Par through a grant managed by the Agence Nationale de la Recherche (ANR), as part of the program "Investissements d'Avenir" under the reference ANR-11-IDEX-0004-02. H.B.'s work has been supported by CNES through the grant "Allocations de recherche postdoctorale." Data are publicly available from the MMS Science Data Center at http://lasp.colorado.edu/mms/sdc/. The French involvement (SCM) on MMS is supported by CNES and CNRS.

References

Alexandrova, O., C. Lacombe, and A. Mangeney (2008), Spectra and anisotropy of magnetic fluctuations in the Earth's magnetosheath: Cluster observations, *Ann. Geophys.*, *26*, 3585–3596.

Buneman, O. (1958), Instability, turbulence, and conductivity in current-carrying plasma, *Phys. Rev. Lett.*, *1*, 119.

Burch, J. L., T. E. Moore, R. B. Torbert, and B. L. Giles (2015), Magnetospheric Multiscale overview and science objectives, *Space Sci. Rev.*, doi:10.1007/s11214-015-0164-9.

Chasapis, A., et al. (2015), Thin current sheets and associated electron heating in turbulent space plasma, *Astrophys. J. Lett.*, *804*, 1.

Dunlop, M. W., A. Balogh, K.-H. Glassmeier, and P. Robert (2002), Four-point Cluster application of magnetic field analysis tools: The curlometer, *J. Geophys. Res.*, *107*(A11), 1384, doi:10.1029/2001JA005088.

Eastwood, J. P., D. G. Sibeck, J. A. Slavin, M. L. Goldstein, B. Lavraud, M. Sitnov, S. Imber, A. Balogh, E. A. Lucek, and I. Dandouras (2005), Observations of multiple X-line structure in the Earth's magnetotail current sheet: A Cluster case study, *Geophys. Res. Lett.*, *32*, L11105, doi:10.1029/2005GL022509.

Elphic, R. C. (1995), Observations of flux transfer events: A review, in *Physics of the Magnetopause*, *Geophys. Monogr. Ser.*, vol. 90, edited by P. Song, B. U. Ö. Sonnerup, and M. F. Thomsen, pp. 225–233, AGU, Washington, D. C.

Ergun, R. E., et al. (2014), The axial double probe and fields signal processing for the MMS mission, *Space Sci. Rev.*, doi:10.1007/s11214-014-0115-x.

Fu, H. S., A. Vaivads, Y. V. Khotyaintsev, V. Olshevsky, M. André, J. B. Cao, S. Y. Huang, A. Retinò, and G. Lapenta (2015), How to find magnetic nulls and reconstruct field topology with MMS data?, *J. Geophys. Res. Space Physics*, *120*, 3758–3782, doi:10.1002/2015JA021082.

Fu, H. S., et al. (2016), Identifying magnetic reconnection events using the FOTE method, *J. Geophys. Res. Space Physics*, *121*, 1263–1272, doi:10.1002/2015JA021701.

Fujimoto, K. (2014), Wave activities in separatrix regions of magnetic reconnection, *Geophys. Res. Lett.*, *41*, 2721–2728, doi:10.1002/2014GL059893.

Gary, S. P., and H. Karimabadi (2006), Linear theory of electron temperature anisotropy instabilities: Whistler, mirror, and Weibel, *J. Geophys. Res.*, *111*, A11224, doi:10.1029/2006JA011764.

Gary, S. P., and R. L. Tokar (1985), The electron acoustic mode, *Phys. Fluids*, *28*, 2439, doi:10.1063/1.865250.

Graham, D. B., Y. V. Khotyaintsev, A. Vaivads, and M. André (2016), Electrostatic solitary waves and electrostatic waves at the magnetopause, *J. Geophys. Res. Space Physics*, *121*, 3069–3092, doi:10.1002/2015JA021527.

Hadid, L. Z., F. Sahraoui, K. Kiyani, A. Retino, R. Modolo, P. Canu, A. Masters, and M. K. Dougherty (2015), Nature of the MHD and kinetic scale turbulence in the magnetosheath of Saturn: Cassini observations, *Astrophys. J. Lett.*, *813*(2), L29.

Huang, S. Y., et al. (2012a), Electron acceleration in the reconnection diffusion region: Cluster observations, *Geophys. Res. Lett.*, *39*, L11103, doi:10.1029/2012GL051946.

Huang, S. Y., M. Zhou, X. H. Deng, Z. G. Yuan, Y. Pang, Q. Wei, W. Su, H. M. Li, and Q. Q. Wang (2012b), Kinetic structure and wave properties associated with sharp dipolarization front observed by Cluster, *Ann. Geophys.*, *30*, 97–107, doi:10.5194/angeo-30-97-2012.

Huang, S. Y., F. Sahraoui, X. H. Deng, J. S. He, Z. G. Yuan, M. Zhou, Y. Pang, and H. S. Fu (2014a), Kinetic turbulence in the terrestrial magnetosheath: Cluster observations, *Astrophys. J. Lett.*, *789*, L28, doi:10.1088/2041-8205/789/2/L28.

Huang, S. Y., et al. (2014b), Observation of directional change of core field inside flux ropes within one reconnection diffusion region in the Earth's magnetotail, *Chin. Sci. Bull.*, *59*(34), 4797–4803.

Huang, S. Y., et al. (2016), In situ observations of flux rope at the separatrix region of magnetic reconnection, *J. Geophys. Res. Space Physics*, *121*, 205–213, doi:10.1002/2015JA021468.

Jovanovic, D., and P. K. Shukla (2004), Solitary waves in the Earth's magnetosphere: Nonlinear stage of the lower-hybrid Buneman instability, *Geophys. Res. Lett.*, *31*, L05805, doi:10.1029/2003GL018047.

Karimabadi, H., et al. (2013), Coherent structures, intermittent turbulence, and dissipation in high-temperature plasmas. *Phys. Plasmas 20*, 012303.

Karimabadi, H., et al. (2014), The link between shocks, turbulence, and magnetic reconnection in collisionless plasmas, Phys. *Plasmas*, *21*, 062308, doi:10.1063/1.4882875.

Khotyaintsev, Y. V., A. Vaivads, M. André, M. Fujimoto, A. Retinó, and C. J. Owen (2010), Observations of slow electron holes at a magnetic reconnection site, *Phys. Rev. Lett.*, *105*, 165002, doi:10.1103/PhysRevLett.105.165002.

Le Contel, O., et al. (2014), The search-coil magnetometer for MMS, *Space Sci. Rev.*, doi:10.1007/s11214-014-0096-9.

Lindqvist, P.-A., et al. (2014), The spin-plane double probe electric field instrument for MMS, *Space Sci. Rev.*, *199*, 1–29, doi:10.1007/s11214-014-0116-9.

Lucek, E. A., D. Constantinescu, M. L. Goldstein, J. Pickett, J. L. Pinçon, F. Sahraoui, R. A. Treumann, and S. N. Walker (2005), The magnetosheath, *Space Sci. Rev.*, *118*, 95–152, doi:10.1007/s11214-005-3825-2.

Omura, Y., H. Matsumoto, T. Miyake, and H. Kojima (1996), Electron beam instabilities as generation mechanism of electrostatic solitary waves in the magnetotail, *J. Geophys. Res.*, *101*, 2685–2697, doi:10.1029/95JA03145.

Phan, T. D., G. Paschmann, C. Twitty, F. Mozer, J. Gosling, J. Eastwood, M. Oieroset, H. Reme, and E. Lucek (2007), Evidence for magnetic reconnection initiated in the magnetosheath, *Geophys. Res. Lett.*, *34*, L14104, doi:10.1029/2007GL030343.

Pickett, J. S., et al. (2003), Solitary potential structures observed in the magnetosheath by the Cluster spacecraft, *Nonlinear Proc. Geophys.*, *11*, 183–196.

Pickett, J. S., et al. (2005), On the generation of solitary waves observed by Cluster in the near-Earth magnetosheath, *Nonlinear Process Geophys.*, *12*, 181–193.

Pollock, C., et al. (2016), Fast Plasma Investigation for Magnetospheric Multiscale, *Space Sci. Rev.*, doi:10.1007/s11214-016-0245-4.

Retinò, A., D. Sundkvist, A. Vaivads, F. Mozer, M. André, and C. J. Owen (2007), In situ evidence of magnetic reconnection in turbulent plasma, *Nature Phys.*, *3*, 236–238.

Roux, A., P. Robert, D. Fontaine, O. Le Contel, P. Canu, and P. Louarn (2015), What is the nature of magnetosheath FTEs?, *J. Geophys. Res. Space Physics*, *120*, 4576–4595, doi:10.1002/2015JA020983.

Roytershteyn, V., W. Daughton, H. Karimabadi, and F. S. Mozer (2012), Influence of the lower-hybrid drift instability on magnetic reconnection in asymmetric configurations, *Phys. Rev. Lett. 108*, 185001.

Roytershteyn, V., Karimabadi H., and Roberts A.. (2015), Generation of magnetic holes in fully kinetic simulations of collisionless turbulence. *Phil. Trans. R. Soc. A 373*, 20140151.

Russell, C. T., et al. (2014), The Magnetospheric Multiscale magnetometers, *Space Sci. Rev.*, doi:10.1007/s11214-014-0057-3.

Sahraoui, F., et al. (2003), ULF wave identification in the magnetosheath: The k-filtering technique applied to Cluster II data, *J. Geophys. Res. 108*(A9), 1335, doi:10.1029/2002JA009587.

Sahraoui, F., G. Belmont, J. L. Pinçon, L. Rezeau, N. Cornilleau-Wehrlin, and A. Balogh (2004), Magnetic turbulent spectra in the magnetosheath: New insights, *Ann. Geophys.*, *22*, 2283–2288.

Sahraoui, F., G. Belmont, L. Rezeau, and N. Cornilleau-Wehrlin (2006), Anisotropic turbulent spectra in the terrestrial magnetosheath as seen by the Cluster spacecraft, *Phys. Rev. Lett.*, *96*, 075002.

Schwartz, S. J., D. Burgess, and J. J. Moses (1996), Low frequency waves in the Earth's magnetosheath: Present status, *Ann. Geophys.*, *14*, 1134–1150.

Shin, K., et al. (2006), Electrostatic quasi-monochromatic waves in the downstream region of the Earth's bow shock based on Geotail observations, *Earth Planets Space*, *58*, 1–7.

Slavin, J. A., et al. (2003a), Geotail observations of magnetic flux ropes in the plasma sheet, *J. Geophys. Res.*, *108*(A1), 1015, doi:10.1029/2002JA009557.

Slavin, J. A., et al. (2003b), Cluster four spacecraft measurements of small traveling compression regions in the near-tail, *Geophys. Res. Lett.*, *30*(23), 2208, doi:10.1029/2003GL018438.

Sonnerup, B. U. O., and M. Scheible (1998), Minimum and maximum variance analysis, in Analysis Methods for Multi-Spacecraft Data, edited by G. Paschmann and P. W. Daly, no. SR-001 in ISSI Scientific Reports, Chap. 1, pp. 185-220, ESA Publ. Div., Noordwijk, Netherlands.

Torbert, R. B., et al. (2014), The FIELDS instrument suite on MMS: Scientific objectives, measurements, and data products, *Space Sci. Rev.*, doi:10.1007/s11214-014-0109-8.

Walsh, A. P., A. N. Fazakerley, R. J. Wilson, I. V. Alexeev, P. D. Henderson, C. J. Owen, E. Lucek, C. Carr, and I. Dandouras (2007), Near-simultaneous magnetotail flux rope observations with Cluster and Double Star, *Ann. Geophys.*, *25*, 1887–1897.

Zhang, Y., H. Matsumoto, and H. Kojima (1999), Whistler mode waves in the magnetotail, *J. Geophys. Res.*, *104*, 28,633–28,644, doi:10.1029/1999JA900301.

Zhou, M., H. Li, X. Deng, S. Huang, Y. Pang, Z. Yuan, X. Xu, and R. Tang (2014), Characteristic distribution and possible roles of waves around the lower hybrid frequency in the magnetotail reconnection region, *J. Geophys. Res. Space Physics*, *119*, 8228–8242, doi:10.1002/2014JA019978.